Journal of Civil Engineering and Construction 2024;13(3):146-158
https://doi.org/10.32732/jcec.2024.13.3.146

Role of Climatic Cycles on the Duality of Chemical and Physical Modes of Sulfate Attack in Concrete

Iman A.N. Omrani[1], Waldemar Maniukiewicz [2], Marcin Świątkowski[2]

1. Department of Building Materials Physics and Sustainable Design, Lodz University of Technology, 93-590 Lodz, Poland
2. Institute of General and Ecological Chemistry, Lodz University of Technology, 90-924 Lodz, Poland
E-mail: iman.abbasi-nattaj-omrani@dokt.p.lodz.pl; waldemar.maniukiewicz@p.lodz.pl; marcin.swiatkowski@p.lodz.pl

Received: 20 May 2024; Accepted: 23 June 2024; Available online: 15 July 2024

Abstract: The possibility of the synergic occurrence of the chemical and physical modes of sulfate attack at the evaporating front is one of the un-resolved issues concerning the case of the partially immersed concretes. Some of the past studies put the accent on chemical sulfate attack as the dominant mechanism, while others identified physical sulfate attack responsible for the degradation of the evaporating front. To fill out this knowledge gap and distinguish the dominant mechanism at work, the presented study focused on the role of climatic condition. Accordingly, visual characteristics, phase composition, and ultrasonic pulse velocity of the immersed and upper-dry regions of the partially immersed concretes in Na_2SO_4 solution were analyzed under different climatic cycles. The designed cycles offered low and high evaporation rates, allowing the thenardite/mirabilite transitions in the $Na_2SO_4.nH_2O$ system. It was found that regardless of the evaporation rate, the mechanisms of physical sulfate attack were favored over the chemical ones. Furthermore, the differences in the evaporation rates of the environments determined the location of the physical sulfate attack. Under high evaporation rate, such aggression was realized beneath the mortar layer of the concrete, leading to its internal microcracking and spalling.
Keywords: Physical sulfate attack; Chemical sulfate attack; Partial immersion; Climatic cycle; Evaporation rate.

1. Introduction

In the early 20th century, the chemical mode of sulfate attack (CSA) was recognized in cementitious materials, and accordingly, various resistant cements were introduced in the building materials industry [1, 2]. Since then, a relatively rich literature has been developed on the topic of CSA, and a standardized test was designed to assess the performance of cementitious systems against this threat [3-5].

Meanwhile, the physical mode of sulfate attack (PSA) was often neglected or mis-identified [6]. PSA refers to the phase transitions of the sulfated salts (particularly $Na_2SO_4.nH_2O$) inside the pores of the cementitious materials which induces an expansive crystallization pressure, leading to their spalling and surface scaling [7]. Unlike CSA, no chemical interactions between the sulfate ions and cement hydrates are at work in the mechanisms of PSA. So far on several field investigations, signs of PSA have been identified within the failed sulfated concrete structures [8-10]. Such observations encouraged the addition of a new chapter, entitled “physical sulfate attack”, in the ACI 201.2R-08: Guide to Durable Concrete [11].

From then on, increasing attention was dedicated to gaining a deeper understanding of the mechanisms of PSA. This has made the “partially immersed concrete in sulfate solution” an special case of interest. In service fields, many concrete structures can be recalled that are partially immersed in sulfated sources, including marine structures, basement walls in residential or industrial areas, abutments, and so forth [6, 12, 13]. In this mode of exposure, the bottom part of the cementitious material is fully immersed in sulfated sources, while its upper section experiences humid air. Sulfate solution ascends toward the upper-dry section of the material via capillary suction. There, an interface forms between the ascended pore solution and the air, where the pore solution finds the chance to evaporate [14, 15]. Since sulfate ions cannot evaporate, they begin to accumulate and form a high concentrated zone near the noted pore solution-vapour interface. The location of this zone is a function of the evaporation rate (J_E) and capillary suction (J_c) as [16, 17]:

$$J_c = \frac{\kappa}{\eta}\frac{(-P_c-\rho_s g h)}{h} \quad (1)$$

where κ is the material's permeability, ρ_s is the pore solution's density, h is the height of the capillary suction, P_c refers to the capillary pressure, η is the pore solution's viscosity, and g is the acceleration due to gravity. When $J_c \geq J_E$ the interface remains to the outer surfaces of the material. Once $J_E > J_c$ the interface progresses beneath the outer surface.

So far, several studies tended to the case of the partially immersed cementitious materials in sulfate solution [18-25]. But, there are still substantial knowledge gaps to be noted.

One of the un-resolved issues is the possibility of the synergic occurrence of CSA and PSA within the upper-dry parts of the partially immersed structures. It was hinted earlier that high concentrated sulfate zones appear at the active evaporating front of these structures. As illustrated in fig. 1, such accumulated sulfate ions face a double tendency:

1) They can either reach supersaturation and precipitate the relevant salts, corresponding to the mechanisms of PSA. Or;

2) They can diffuse toward de-stabilizing the existing cement hydrates and contribute to the mechanisms of CSA.

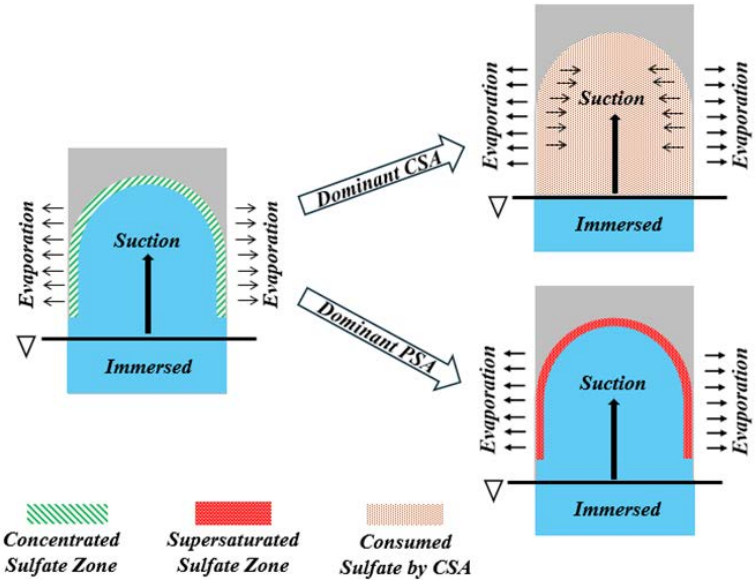

Figure 1. Schematic of the duality of CSA and PSA within the evaporating front of the partially immersed cementitious materials

Regarding the mentioned duality, two different schools of thought have been formed. On the one hand, the authors of [7, 18, 19] put the accent on CSA as the main aggressive mechanism. They reasoned that the mentioned high concentrated zones could accelerate the progress of CSA, and the mechanisms of PSA, if any, became evident after CSA had deteriorated the microstructure. On the other hand, there exist several studies that could not detect any notable signs of CSA in the damaged evaporating front of their samples. Instead, abundant salt crystals were observed there, signifying the PSA as the dominant mechanism at work [9, 12, 20, 25-27].

As discussed, there is no consensus on the main responsible mechanism behind the damage of the evaporating front of the partially immersed concretes in sulfated fields. This knowledge gap is practically important because only after identifying the responsible mechanism, one can think about the possible improvement strategies.

The role of the climatic condition is one of the missing pieces to solve the noted duality. To the best of our knowledge, there is scarce data in the literature focused on this role. The performance of the partially immersed cementitious samples has only been studied under one climatic cycle in the previously cited works [12, 18, 19, 24, 25, 27]. Hence, to fill out this missing piece, it is the objective of the present research to evaluate the duality of CSA & PSA in damaging the partially immersed concretes under different climatic cycles.

2. Experimental

2.1 Materials

The utilized binder for manufacturing the concrete samples was ordinary Portland cement (OPC) type I (CEM I 42.5R) with the chemical composition as detailed in table 1.

Table 1. Chemical composition of the utilized cement.

Oxide	Mass (%)
SiO_2	21.8
Fe_2O_3	2.9
Al_2O_3	5.4
CaO	66.8
MgO	1.5

Natural aggregates were provided from a local river and fell into the following categories; Coarse aggregates with the diameter ranging from 8-16mm, medium aggregates with the diameter of 2-8mm, and sand with the diameter of less than 2mm. Tap water was used for the creation of the concrete mixture. Table 2 details the concrete's mix proportions.

Table 2. Mix proportions of the concrete (kg/m^3).

OPC	Water	Water/OPC	Coarse Aggregate	Medium Aggregate	Sand
390	195	0.5	558	648	594

A laboratory mixer was employed for mixing the ingredients. First, aggregates and cement were mixed for 30s, then while stirring, water was gradually spread throughout the mixture. The mixing process lasted for approx. 5 mins. Upon its completion, the slump consistency and air content of the fresh mixture were measured based on [28, 29] and found out to be 60mm and 3.4%, respectively. Subsequently, the fresh concrete was poured into rectangular prismatic molds with the dimensions of 100x100x200mm. The cast concretes were de-moulded after 24h and moved into a water tank under room temperature to cure for 28 days. After the curing period, concretes were kept under room condition for 1 week. This stage was intended to lower the saturation level of the cured concretes to intensify the following suction of the sulfate solution into them.

2.2 Research plan

In this study, 5% Na_2SO_4 solution was utilized as the sulfated source. To simulate the partial immersion condition in the fields, the cured prismatic OPC concretes were exposed to the solution as displayed in fig. 2.

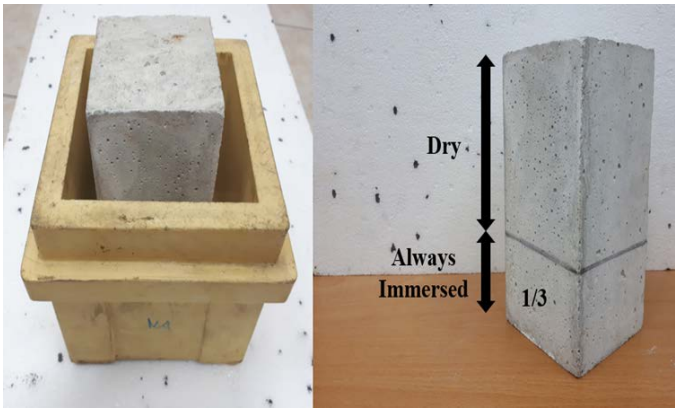

Figure 2. Schematic of the partial immersion condition

As can be seen from fig. 2, the bottom 1/3 of the samples remained permanently immersed in the solution, while the upper 2/3 of the samples was in contact with the air. To make sure that each concrete was exposed to the same amount of solution during the analysis, the prepared solutions were poured into similar 150x150x150mm plastic boxes as shown in fig. 2 to hold each sample solely.

Fig. 3 displays the phase diagram of the $Na_2SO_4.nH_2O$ system.

The simulated climatic cycles of this study were designed in such a way to allow transition between thenardite ($Na_2SO_4(V)$) and mirabilite ($Na_2SO_4.10H_2O$) at the upper 2/3 of the samples based on fig. 3. As signaled in fig. 3, the details of the designed climatic cycles are:

1) E1 ➔ For 1 week, partially immersed concretes were kept under 20°C and RH of 80% (stable presence of mirabilite). Next, while still partially immersed, samples were moved to oven under 40°C and RH of 14% for another week (stable presence of thenardite) to complete one cycle.

2) E2 ➔ For 1 week, partially immersed concretes were kept under 20°C and RH of 36% (stable presence of thenardite). Next, while still partially immersed, samples were moved to refrigerator under 2°C and RH of 75% for another week (stable presence of mirabilite) to complete one cycle.

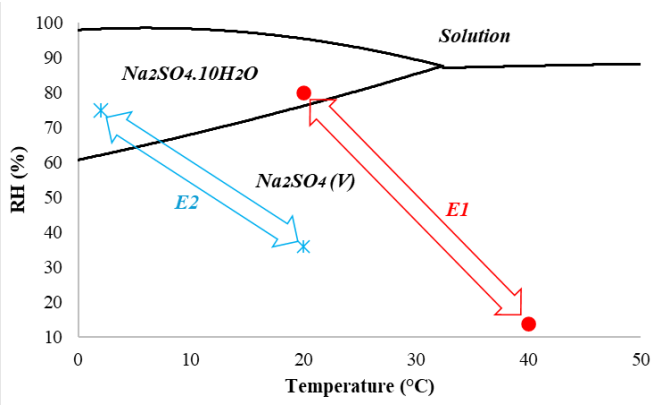

Figure 3. Phase diagram of the Na2SO4.nH2O system, covering the stable phases after [30]

12 cycles were completed in this study. To maintain the level and concentration of the Na_2SO_4 solution throughout the whole project, the solutions were renewed after the completion of each cycle.

The designed environments were inspired by the diurnal climatic fluctuations during the hot and cold seasons. While both E1 and E2 allow the thenardite/mirabilite transitions, they offer respectively high and low evaporation rates.

To identify the responsible deterioration mechanism under the mentioned different environments, the visual characteristics and phase composition of the evaporating front of the samples were assessed. The visual characteristics were recorded every 4 cycles to be compared with each other. After completing the 12 cycles, segments were collected from the mortar layer of the upper 2/3 sections of the samples for the phase composition analyses. Segments were also extracted from their immersed parts (where only CSA was possible) for reference. The sampling depth was down to 10mm from the outer surface and carried out on all 4 faces of the concretes. Sampling was done on at least two concrete samples. The collected segments were divided into two groups; one group was immediately moved for the scanning electron microscopy (SEM) analysis combined with the energy dispersive X-ray spectroscopy (EDS). The other group was ground and passed through a 63µm sieve to separate the quartz from the paste as much as possible for the X-ray diffraction (XRD) and thermogravimetry (TG) investigations.

Furthermore, to follow the microcracking condition of the upper-dry parts of the concretes under the different environments, the non-destructive method of ultrasonic pulse velocity (UPV) was utilized. The UPV measurements were done at the evaporating front of the samples in two-cycle intervals. The UPV measurements were also conducted on the immersed parts of the concretes (where only CSA was possible) for reference.

Fig. 4 presents the diagram of the research plan.

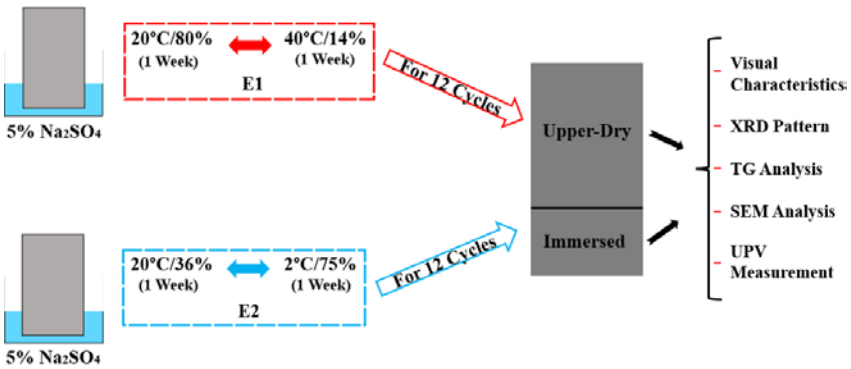

Figure 4. Schematic of the research plan

2.3 Techniques

2.3.1 Visual characteristics

Every 4 cycles, the efflorescence that formed on the concretes was removed gently via a brush, and the visual characteristics of the samples that experienced the different climatic cycles were recorded and compared with one another.

2.3.2 X-ray diffraction pattern

PANalytical X'Pert Pro MPD diffractometer (Malvern Panalytical Ltd., Royston, UK) was utilized to obtain the X-ray diffraction patterns of the samples in the Bragg–Brentano reflection geometry under room temperature. The copper CuKa radiation was used from a sealed tube (30 mA, 40 kV), and the analysis was conducted in the 2θ range of 4–80° with a step of 0.017° and an exposure per step of 200s. To avoid preferred orientation effects, samples were turned around throughout the data collection. PANalytical HighScore software (ver. 4.9, Malvern PANalytical Ltd., Royston, UK) plus the International Centre for Diffraction Data's (ICDD) powder diffraction file (PDF-2 ver. 2020) database of standard reference materials were used to identify the phases. 200-300mg of powdered samples was used for each measurement.

2.3.3 Thermogravimetry

Netzsch STA 449 F1 Jupiter thermos-analyzer was used for the TG analysis. 50mg of powdered sample was heated in an open corundum crucible under 50cm3/min of nitrogen flow. The temperature range of the analysis was 30–1000°C with the heating rate of 20°C/min.

2.3.4 Scanning electron microscopy

Quanta FEG 250 microscope (FEI, Hillsboro, OR, USA), combined with the EDAX (Mahwah, NJ, USA) were utilized for the SEM/EDS investigations. The surfaces of the collected segments were coated by a 50nm carbon layer to provide the required conductivity. The analyses were conducted under a low vacuum condition of 40 Pa.

2.3.5 Ultrasonic pulse velocity

An ultrasonic pulse analyzer (i.e. Controls) equipped with two circular transducers having the diameter of 50mm and the precision of 0.1 μs was used for the non-destructive UPV recording of the upper-dry and immersed parts of the concretes. Each measurement was done on 3 separate samples for averaging.

3. Results

3.1 Visual characteristics

Fig. 5 illustrates the typical conditions of the concrete samples in 4-cycle intervals.

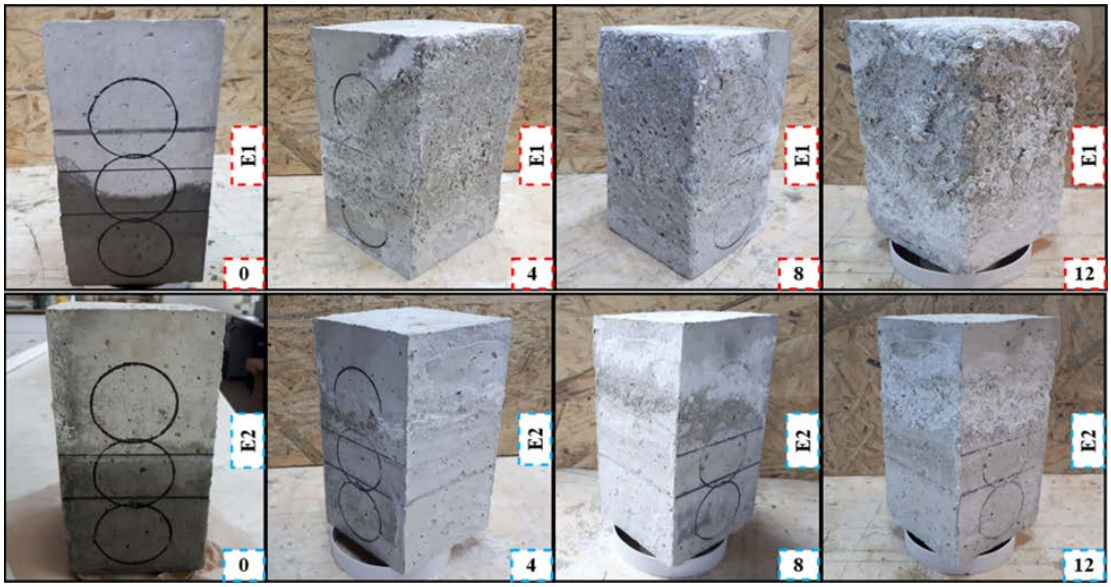

Figure 5. Typical condition of the concretes under the E1 and E2 climates every 4 cycles

As can be followed from fig. 5, the E1 climatic cycle induced a much more severe and faster degradation in the concretes compared with the E2 cycle. The serious surface scaling appeared on the evaporating front of the E1 samples after only 4 cycles. Whereas, the scaling revealed itself under the E2 climatic cycle after approx. 8 cycles with a less intensity. Fig. 6 provides a closer look on the schematic modes of the degradation in the evaporating front of the concretes after completing the 12 cycles.

The typical aftermaths in the evaporating front of the concretes that experienced the E1 climatic cycle were:

1) Complete removal of the surface paste layer,
2) Spalling of the mortar layer,
3) Eventual exposure of the inner coarse aggregates.

In the case of the E2 concretes, the surface paste layer was scaled gradually. But unlike the E1 samples, the mortar layer beneath their surface remained nearly intact and no notable spalling was observed, as shown in fig. 6.

The illustrated scaled regions in figs. 5 and 6 were chosen for the phase composition analyses and UPV measurements as discussed in the up-coming sections.

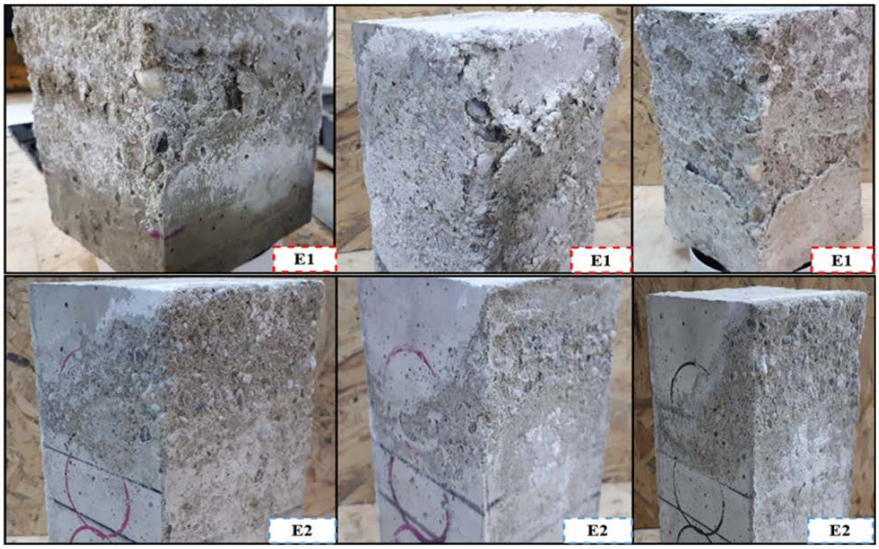

Figure 6. Schematic modes of the degradation in the evaporating front of the concretes under the E1 and E2 climates after 12 cycles

3.2 X-ray diffraction patterns

Fig. 7 displays the XRD patterns of the immersed and upper-dry regions of the concretes under the E1 and E2 climatic cycles in the enlarged 2θ range of 4-40°.

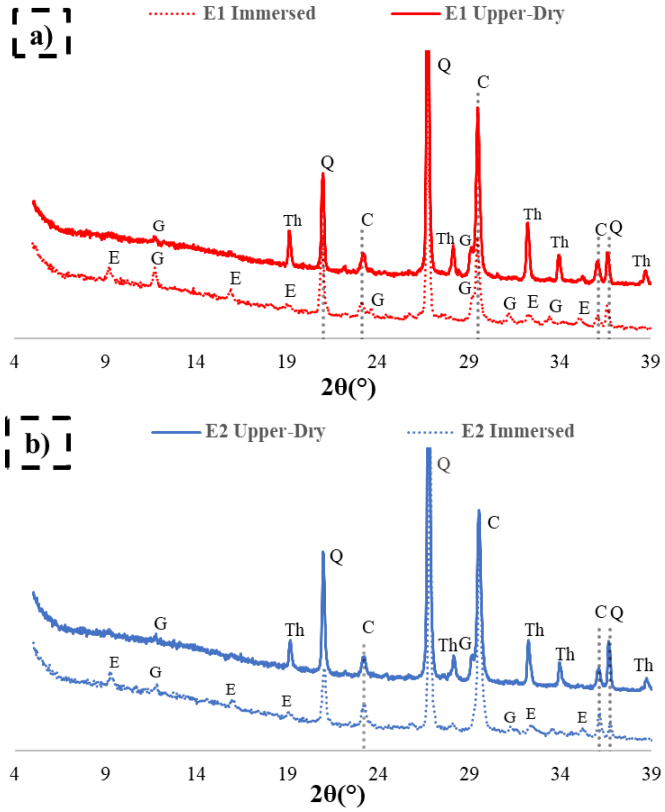

Figure 7. XRD patterns of the immersed and upper-dry sections of the concretes: a) under the E1 climate; b) under the E2 climate (E=Ettringite, G=Gypsum, Th=Thenardite, Q=Quartz, C=Calcite)

Based on figs. 7a and 7b, the typical signs of Na_2SO_4-induced CSA (precipitation of ettringite and gypsum, following the decomposition of portlandite [31]) were expectedly found within the immersed parts of the E1 and E2 samples. However, when it comes to the evaporating front of the concretes, one can see from figs.7a and 7b that no detectable ettringite, with only slight traces of gypsum, could be detected under both E1 and E2 cycles. Instead, evident thenardite maxima appeared there.

3.3 Thermogravimetry analysis

Fig. 8 shows the obtained TG curves from the immersed and upper-dry regions of the E1 and E2 concretes in the temperature range of 50-250°C.

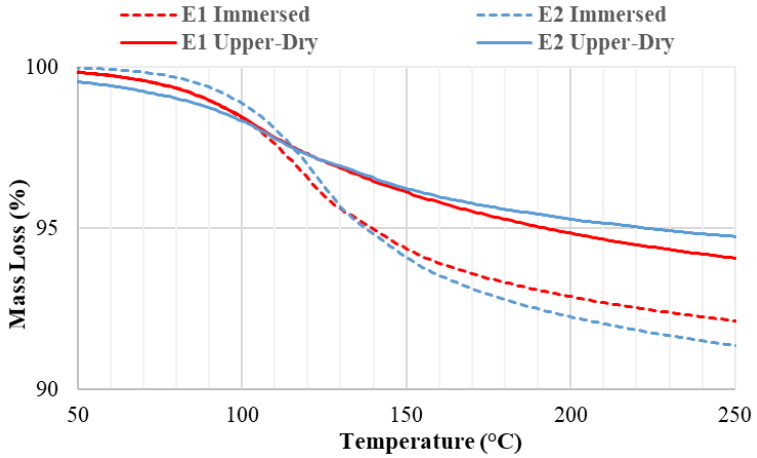

Figure 8. TG curves of the immersed and upper-scaled regions of the E1 and E2 concretes

Throughout the noted temperature range, mass losses due to the following endothermic reactions are expected [32]:

1) De-hydration of the free and adsorbed water on the surface of the hydrates.
2) De-hydration of ettringite.
3) De-hydration of gypsum.
4) Partial de-hydration of the chemically bound water of the C-S-H gel which gradually persists up until 600°C.

Table 3 summarizes the recorded mass losses of fig. 8.

Table 3. Recorded TG mass losses in the temperature range of 50-250°C

Sample	E1 Immersed	E1 Upper-Dry	E2 Immersed	E2 Upper-Dry
Mass Loss (%)	92.14	94.07	91.37	94.76

According to fig. 8 and table 3, 32.5% & 64.6% higher mass losses were recorded within the immersed sections of the E1 and E2 samples, respectively, compared with their upper-dry parts. To identify the de-hydrated phases in fig. 8, fig. 9 displays the differential TG curves.

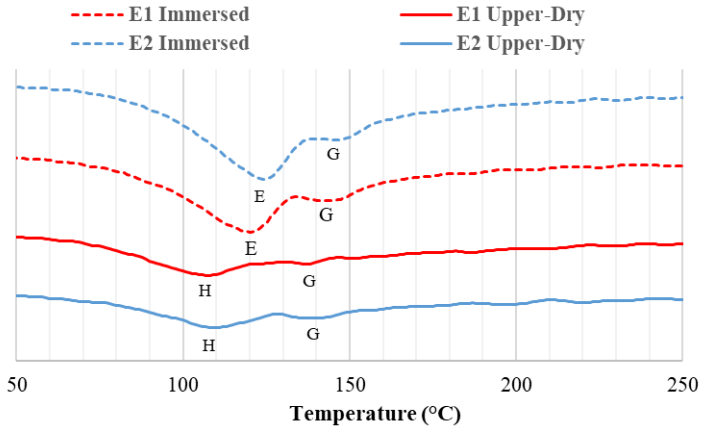

Figure 9. Differential TG curves of the immersed and upper-scaled regions of the E1 and E2 concretes (H=C-S-H gel, E=Ettringite, G=Gypsum)

Based on fig. 9, the immersed parts of the E1 and E2 concretes revealed two maxima at approx. 123°C and 141°C, which can be assigned to the de-hydration of ettringite [33] and gypsum [32], respectively. Within the evaporating front of both samples, the first peak shifted to lower temperatures at approx. 107°C, corresponding to the partial de-hydration of C-S-H gel [34]. This peak was masked in the immersed parts due to the intense presence of ettringite. The second peak in both E1 and E2 evaporating fronts appeared at approx. 138°C, assigning to the gypsum dehydration. But, the intensity of this peak was lower than that of the immersed regions.

Combining such phase identifications with fig. 8 and table 3, one infers the intense presence of the CSA products inside the immersed sections of both samples. However, within their evaporating fronts, no notable ettringite and slight gypsum could be detected. This agrees with the observations of section 3.2.

3.4 Scanning electron microscopy

To provide a more detailed view on the upper-dry microstructure of the concretes under the E1 and E2 cycles, SEM/EDS analysis was utilized. Figs. 10 and 11 display different locations from the upper-dry microstructure under the E1 climatic cycle.

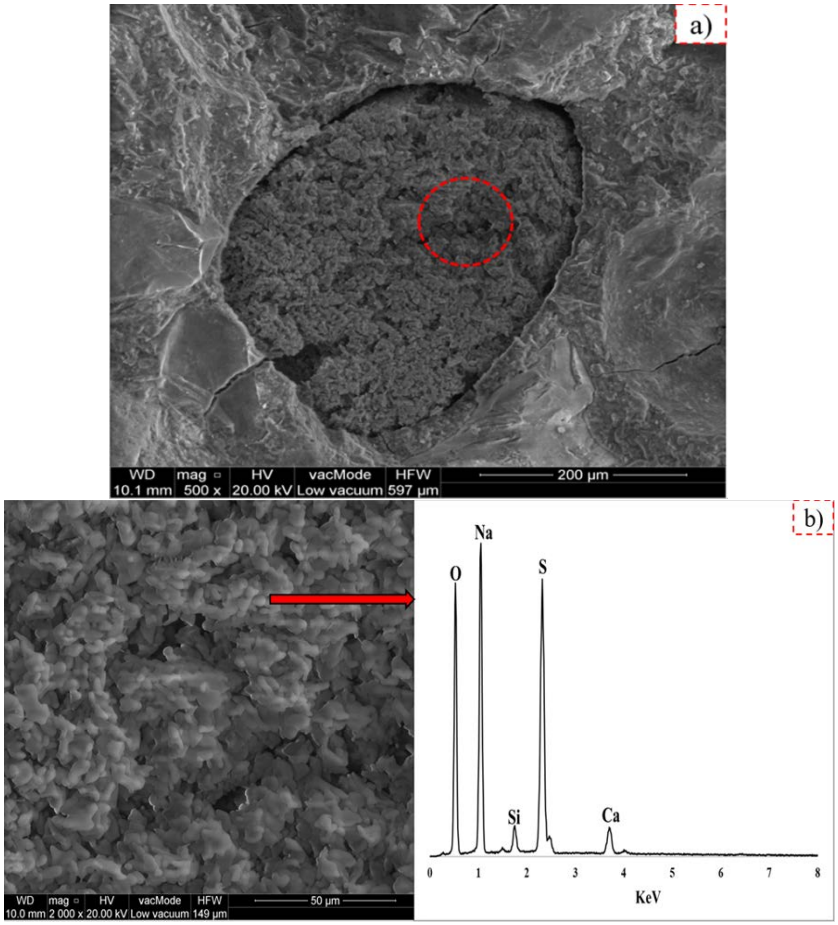

Figure 10. Upper-dry microstructure of the concrete under the E1 climate: a) detection of a filled pore with adjacent microcracks, b) identifying thenardite inside the pore (S=Sulfate, Si=Silicate, Na=Sodium, Ca=Calcium)

As can be seen from figs. 10 and 11, filled pores with pseudo-spherical substances were detected at the evaporating front of the samples under the E1 climate. Based on the conducted EDS analysis, abundant sulfate and sodium ions were found within the noted pores. Such features, in agreement with the findings of section 3.2, indicate that the pores were filled with thenardite.

Figs. 12 and 13 illustrate various locations from the upper-dry microstructure under the E2 climatic cycle.

Based on fig. 12, precipitated thenardite were detected on the surface of the aggregates under the E2 climate. In addition, pseudo-columnar phases were seen there, as shown in fig. 13. From a closer perspective, EDS analysis detected abundant calcium and sulfate ions within such phases, identifying them as gypsum crystals in agreement with the observations of the sections 3.2 and 3.3.

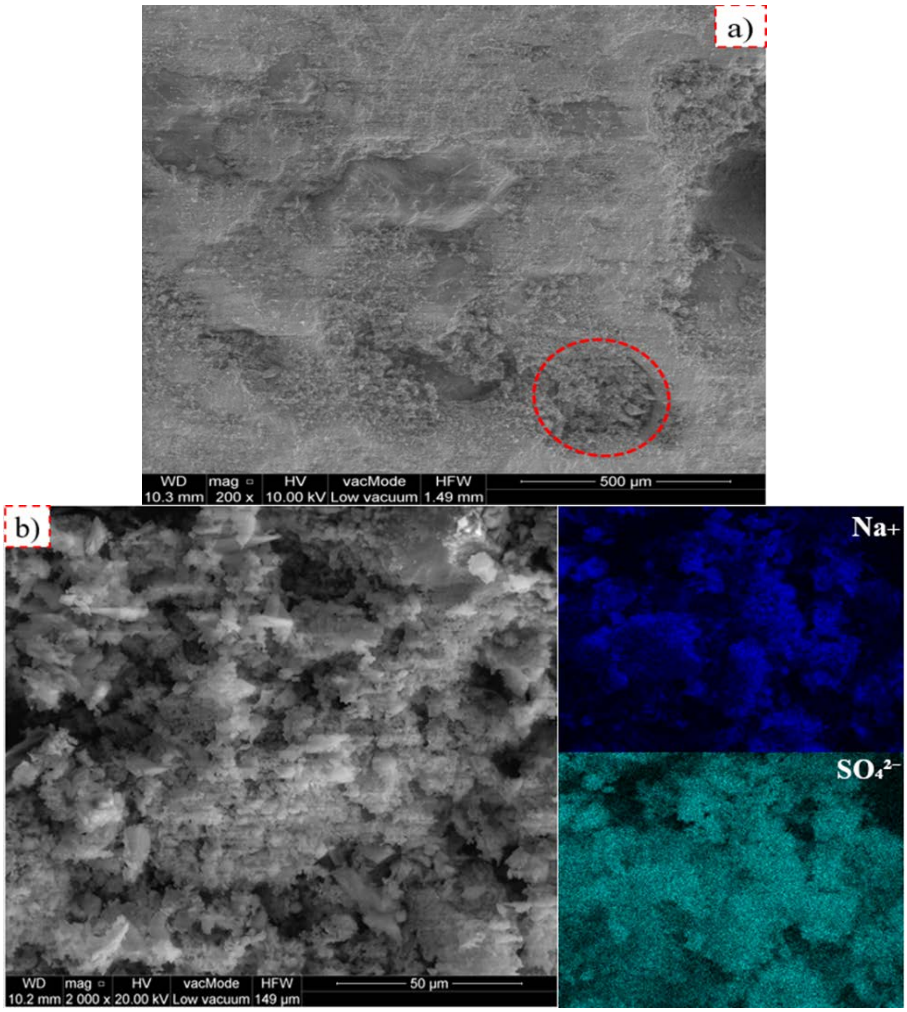

Figure 11. Upper-dry microstructure of the concrete under the E1 climate: a) detecting a filled gap, b) identifying thenardite through mapping sodium and sulfate ions within the gap

3.5 Ultrasonic pulse velocity

Fig. 14 shows the average UPV measurements of the immersed and upper-dry sections of the E1 and E2 concretes.

Based on fig. 14, the most notable drop of the average UPV was recorded at the upper-dry parts of the E1 concretes. There, the highest reduction (i.e. for approx. 6%) occurred between the 6-8 cycles. This is in accordance with the observations of section 3.1, where during the mentioned period, nearly all the paste layer of the E1 upper-dry parts was scaled. Figs. 5 and 6 already presented that between the 10-12 cycles, the upper mortar layer of the E1 concretes also spalled. Because of such spalling and lack of the smooth surface, the UPV measurements could not be done during the noted period. Concerning the upper-dry parts of the E2 concretes, one notes that the average UPV evolved with the same pattern as the immersed regions of the samples.

Unlike the sudden drop of the UPV at the upper-dry parts of the E1 samples, the immersed parts revealed a gradual and less intense drop between the 6-12 cycles. There, the average UPV decreased for approx. 3.5 and 5% at the immersed parts of E1 and E2 samples, respectively.

3.6 Discussions

Based on the presented observations, while the typical products of the Na_2SO_4-induced CSA appeared inside the immersed parts of the concretes after 6 months, no detectable ettringite with only slight traces of gypsum could be found within their evaporating fronts. Thus, the role of CSA in deteriorating the upper-dry regions of the concretes can be excluded. Instead, abundant thenardite was witnessed there, plus the typical aftermaths of salt weathering (i.e. surface scaling & spalling as shown in section 3.1.). Accordingly, one infers that the main role behind the failure of the evaporating front of the concretes was PSA.

This is in contrast with those studies that detected CSA as the main damaging mechanism in the upper-dry regions of their samples [7, 18, 19]. The key note here is that the partially immersed samples of [18, 19] were

stored under a constant temperature and RH. Presumably, under such constant climatic condition, the concentrated Na^+ and SO_4^{2-} ions at the evaporating front find the chance to diffuse toward reacting with the cement hydrates. But, as presented in this work, in case of the climatic cycles that allow the thenardite/mirabilite transition (no matter the evaporation rate), the noted concentrated ions rather made the pore solution supersaturated and contributed to the mechanisms of PSA.

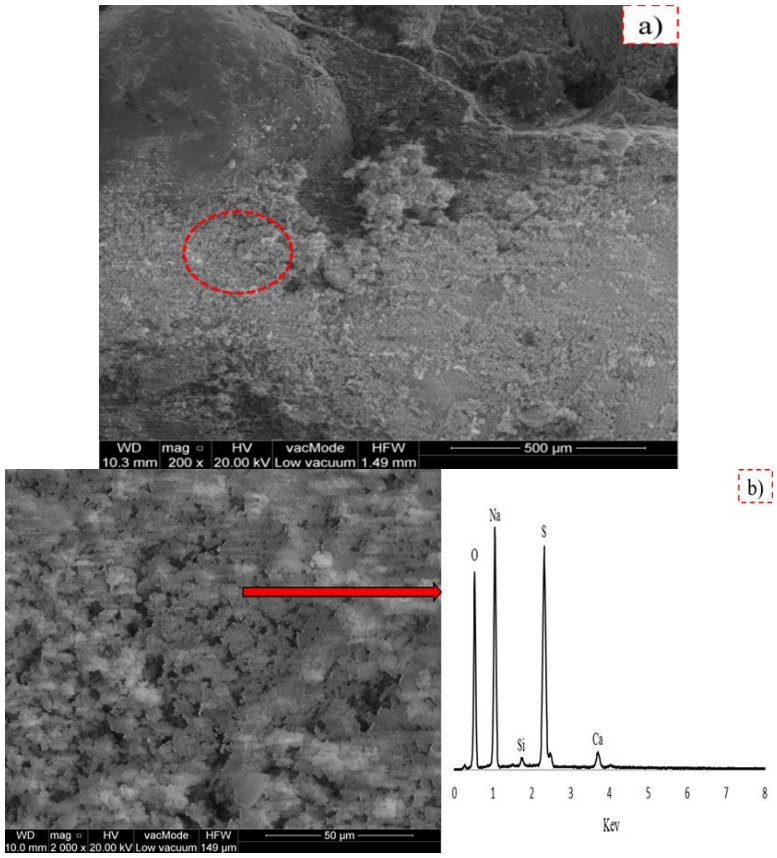

Figure 12. Upper-dry microstructure of the concrete under the E2 climate: a) detection of the precipitated phases on the aggregate's surface, b) identifying the thenardite crystals (S=Sulfate, Na=Sodium, Ca=Calcium, Si=Silicate)

This tendency can be explained considering the kinetics of the undergoing processes. More time is required for the de-stabilization of the paste's hydrates and involvement of the sulfate ions in CSA. Whereas, crystallization of the relevant $Na_2SO_4.nH_2O$ salts upon supersaturation can be an immediate phenomenon. Such difference elaborates why only little gypsum could be detected in the upper-dry regions, while the presence of thenardite was plentiful.

It is remarkable that PSA was the dominant tendency under both climatic cycles. The probable mechanism of PSA in this work was the precipitation of thenardite under the E1 and E2 climates when RH was equal to 14% and 36%, respectively. The subsequent rise of RH (and cooling of the temperature) to 75% and 80% led to the dissolution of such thenardite. This event highly supersaturated the pore solution with respect to mirabilite, having a 314% higher molar volume than that of the thenardite, and induced it's through-solution crystallization [35]. The mentioned cyclic transition applied pressure upon the pore walls which surpassed the tensile strength of the concretes, leading to their microcracking [36] (see fig. 10).

Although the same PSA mechanism occurred under the E1 and E2 climatic cycles, the location of the concrete's evaporating front was different. As observed in section 3.1., the upper-dry mortar layer of the concretes that underwent the E1 cycle received a significant spalling. Whereas, the concretes that experienced the E2 cycle maintained their mortar layer, receiving only the scaling of their exterior paste layer. This difference is due to the higher evaporation rate offered by the E1 climatic cycle than that of the E2 one. The evaporation rate offered by the E1 climatic cycle exceeded the capillary suction rate (see Eq. (1)) above the immersion line, and thus, formed the pore solution/air interface below the mortar layer of the samples. Consequently, the crystallization pressure was applied upon the mortar layer and spalled it [37]. Analogously, the most sudden and sever drop in the average UPV was recorded at the upper-dry parts of the E1 concretes (see fig. 14), which can be attributed to the internal microcracking and spalling of their mortar layer. In the case of the E2 cycle, such interface was created above the

mortar layer, and thus, put its pressure only upon the exterior paste layer of the samples. Fig. 15. illustrates the schematic mechanism of PSA under the E1 and E2 climatic cycles.

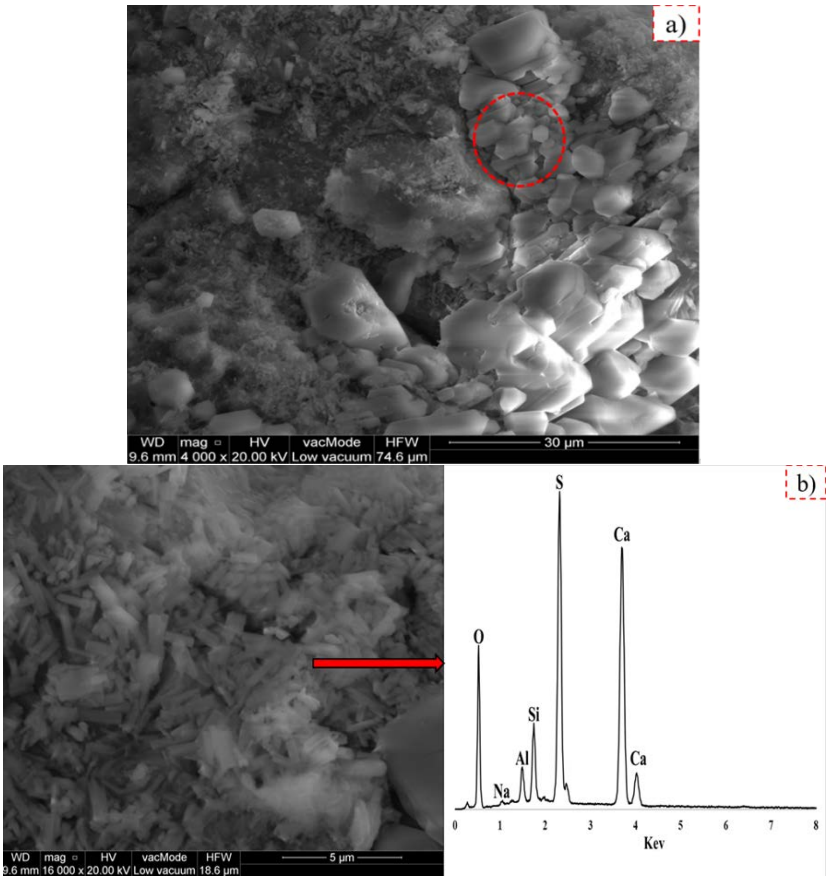

Figure 13. Upper-dry microstructure of the concrete under the E2 climate: a) detection of pseudo-columnar phases, b) identifying the gypsum crystals (S=Sulfate, Na=Sodium, Ca=Calcium, Si=Silicate, Al=Aluminate)

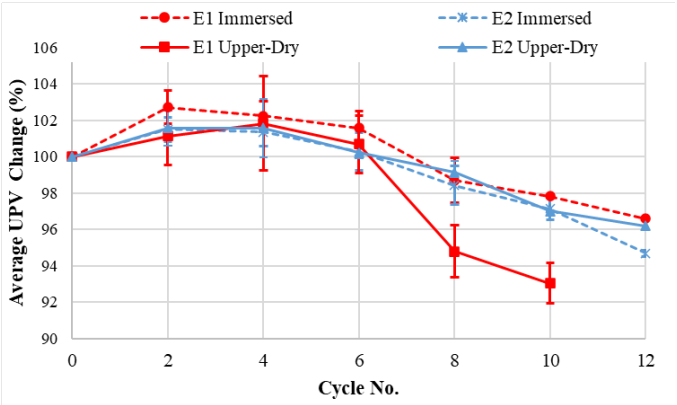

Figure 14. Average UPV measurements of the immersed and upper-dry sections of the concretes under the E1 and E2 climatic cycles

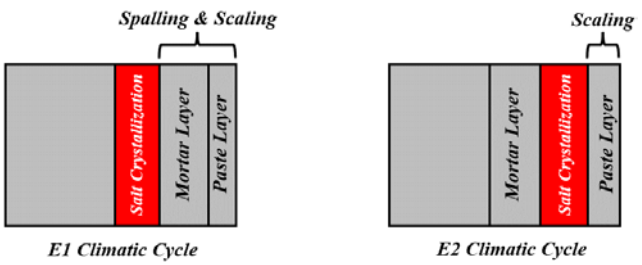

Figure 15. Schematic of the PSA mechanism at the evaporating front of the concretes under the E1 and E2 climates

4. Conclusions

The presented study investigated the duality of CSA and PSA at the evaporating front of the partially immersed OPC concretes in Na_2SO_4 solution. The objective was to distinguish the dominant aggressive mechanism there under different climatic cycles offering high and low evaporation rates. Both climatic cycles were designed in such a way to induce the thenardite/mirabilite transition. After 6 months of exposure, the followings were noted:

1) The evaporating front of the concretes that experienced the low evaporation rate cycle received scaling of their outer paste layer.

2) The concretes that were subjected to high evaporation rate cycle not only got paste scaling, but also spalling of their beneath mortar layer.

3) The fully immersed sections of the concretes were filled with the Na2SO4-induced CSA products. However, no detectable ettringite with slight traces of gypsum were found within their evaporating fronts. This situation was encountered under both climatic cycles.

4) Abundant thenardite was witnessed within the evaporating front of the concretes. These salts precipitated mostly on the aggregate's surfaces, filling the microstructural pores and pressuring the surrounding skeletons, leading to their microcracking.

5) The UPV of the evaporating from of the concretes that underwent the high evaporation rate cycle dropped suddenly and intensely, analogous to the initiation of the mortar spalling. Compared with it, the UPV of the immersed parts of the samples (no matter the evaporation rate) decreased gradually and less intensely.

Based on the above notes, it can be concluded that under the climatic fluctuations which allow the thenardite/mirabilite transition (no matter the low or high evaporation rate), the accumulated Na^+ and SO_4^{2-} ions at the evaporating front of the concretes preferably crystallize upon supersaturation, rather than being consumed by CSA. Thus, PSA can be distinguished as the main mechanism behind the deterioration of the upper-dry regions of such structures.

Under high evaporation rate, the mentioned salt transitions occurred beneath the mortar layer of the concrete and thus, spalled it. There, internal microcracks appeared at the mortar layer which notably dropped the average UPV (i.e. for approx. 8%). However, under low evaporation rate, such crystallizations were near the outer paste layer, causing only the exterior surface scaling and preserving the mortar layer.

It was pointed out that the previous studies which put the accent on the role of CSA in damaging the evaporating front of the cementitious materials were conducted under constant temperature and RH. Based on the findings of the present study, however, the mere chance of thenardite/mirabilite phase transition made the mechanisms of PSA kinetically favorable over CSA.

Acknowledgement

The publication was produced as part of the Doctoral Candidate's (i.e. First author) participation in a project of the National Agency for Academic Exchange within the framework of the "STER" Programme. - Internationalisation of Doctoral Schools" as part of the project "Curriculum for advanced doctoral education & training - CADET Academy of Lodz University of Technology.

5. References

[1] Massaad G, Rozière E, Loukili A, Izoret L. Advanced testing and performance specifications for the cementitious materials under external sulfate attacks. Construction and Building Materials. 2016;127:918-931.

[2] Alyami MH, Alrashidi RS, Mosavi H, Almarshoud MA, Riding KA. Potential accelerated test methods for physical sulfate attack on concrete. Construction and Building Materials. 2019;229:116920.

[3] American Society for Testing Materials, ASTM C1012/C1012M – Standard Test Method for Length Change of Hydraulic-Cement Mortars Exposed to a Sulfate Solution. ASTM International, West Conshohocken, PA, 2012.

[4] Wang B, Li G, Panesar DK. A study of variables that affect the process of sulfate attack of cement-based materials subjected to stray current. Structural Concrete. 2022;23(2):706-721.

[5] Chen H, Huang H, Qian C. Study on the deterioration process of cement-based materials under sulfate attack and drying-wetting cycles. Structural Concrete. 2018;19(4):1225-1234.

[6] Haynes H, O'Neill R, Mehta PK. Concrete deterioration from physical attack by salts. Concrete International. 1996;18(1):63-68.

[7] Liu Z, Deng D, De Schutter G. Does concrete suffer sulfate salt weathering?. Construction and Building Materials. 2014;66:692-701.

[8] Al-Amoudi OS. Attack on plain and blended cements exposed to aggressive sulfate environments. Cement and Concrete Composites. 2002;24(3-4):305-316.

[9] Yoshida N, Matsunami Y, Nagayama M, Sakai E. Salt weathering in residential concrete foundations exposed to sulfate-bearing ground. Journal of Advanced Concrete Technology. 2010;8(2):121-134.
[10] Novak GA, Colville AA. Efflorescent mineral assemblages associated with cracked and degraded residential concrete foundations in Southern California. Cement and Concrete Research. 1989;19(1):1-6.
[11] ACI committee web letter: 201.2R. Physical salt attack; 2010 [chapter 8].
[12] Sakr MR, Bassuoni MT. Performance of concrete under accelerated physical salt attack and carbonation. Cement and Concrete Research. 2021;141:106324.
[13] Haynes H, Bassuoni MT. Physical salt attack on concrete. Concrete international. 2011;33(11):38-42.
[14] Hall MR, Allinson D. Evaporative drying in stabilized compressed earth materials using unsaturated flow theory. Building and environment. 2010;45(3):509-518.
[15] Liu Z, Deng D, De Schutter G, Yu Z. Chemical sulfate attack performance of partially exposed cement and cement+ fly ash paste. Construction and Building Materials. 2012;28(1):230-237.
[16] Muskat M, Meres MW. The flow of heterogeneous fluids through porous media. Physics. 1936;7(9):346-363.
[17] Bear J. Dynamics of fluids in porous media. Courier Corporation; 2013 Feb 26.
[18] Liu Z, De Schutter G, Deng D, Yu Z. Micro-analysis of the role of interfacial transition zone in “salt weathering” on concrete. Construction and Building Materials. 2010;24(11):2052-2059.
[19] Liu Z, Deng D, De Schutter G, Yu Z. Micro-analysis of “salt weathering” on cement paste. Cement and Concrete Composites. 2011;33(2):179-191.
[20] Bassuoni MT, Nehdi ML. Durability of self-consolidating concrete to different exposure regimes of sodium sulfate attack. Materials and Structures. 2009;42:1039-1057.
[21] Liu P, Chen Y, Wang W, Yu Z. Effect of physical and chemical sulfate attack on performance degradation of concrete under different conditions. Chemical physics letters. 2020;745:137254.
[22] Zhao G, Guo M, Cui J, Li J, Xu L. Partially-exposed cast-in-situ concrete degradation induced by internal-external sulfate and magnesium multiple coupled attack. Construction and Building Materials. 2021;294:123560.
[23] Irassar EF, Di Maio A, Batic OR. Sulfate attack on concrete with mineral admixtures. Cement and Concrete Research. 1996;26(1):113-123.
[24] Bassuoni MT, Rahman MM. Response of concrete to accelerated physical salt attack exposure. Cement and concrete research. 2016;79:395-408.
[25] Nehdi M, Hayek M. Behavior of blended cement mortars exposed to sulfate solutions cycling in relative humidity. Cement and Concrete Research. 2005;35(4):731-742.
[26] Esselami R, Wilson W, Tagnit-Hamou A. An accelerated physical sulfate attack test using an induction period and heat drying: First applications to concrete with different binders including ground glass pozzolan and limestone filler. Construction and Building Materials. 2022;345:128046.
[27] Nehdi ML, Suleiman AR, Soliman AM. Investigation of concrete exposed to dual sulfate attack. Cement and Concrete Research. 2014;64:42-53.
[28] ASTM C143/C143M-12, Standard Test Method for Slump of Hydraulic-Cement Concrete. ASTM International, 2012.
[29] ASTM C231-08c, Standard Test Method for Air Content of Freshly Mixed Concrete by the Pressure Method, 2008.
[30] Rodriguez-Navarro C, Doehne E, Sebastian E. How does sodium sulfate crystallize? Implications for the decay and testing of building materials. Cement and concrete research. 2000;30(10):1527-1534.
[31] J. Marchand, J.P. Ivan Older, Skalny. Sulfate Attack on Concrete (Modern Concrete Technology), Spon Press, London and New York, 2002.
[32] Scrivener K, Snellings R, Lothenbach B, Press CR, editors. A practical guide to microstructural analysis of cementitious materials. Boca Raton, FL, USA: CRC Press; 2016.
[33] Villagrán-Zaccardi YA, Egüez-Alava H, De Buysser K, Gruyaert E, De Belie N. Calibrated quantitative thermogravimetric analysis for the determination of portlandite and calcite content in hydrated cementitious systems. Materials and Structures. 2017;50:1-10.
[34] Skaropoulou A, Tsivilis S, Kakali G, Sharp JH, Swamy RN. Long term behavior of Portland limestone cement mortars exposed to magnesium sulfate attack. Cement and Concrete Composites. 2009;31(9):628-636.
[35] Thaulow N, Sahu S. Mechanism of concrete deterioration due to salt crystallization. Materials Characterization. 2004;53(2-4):123-127.
[36] Flatt RJ, Steiger M, Scherer GW. A commented translation of the paper by CW Correns and W. Steinborn on crystallization pressure. Environmental geology. 2007;52(2):187-203.
[37] Scherer GW. Stress from crystallization of salt. Cement and concrete research. 2004;34(9):1613-1624.